Interaction of a Peptide Derived from the N-Heptad Repeat Region of gp41 Env Ectodomain with Model Membranes. Modulation of Phospholipid Phase Behavior†

Roberto Pascual,‡ Mariela Contreras,§ Alexander Fedorov,|| Manuel Prieto,|| and José Villalaín*,‡

Instituto de Biología Molecular y Celular, Universidad "Miguel Hernández", E-03202 Elche-Alicante, Spain, Facultad de Ciencias y Tecnología, Universidad de Carabobo, Valencia, Venezuela, and Centro de Química-Física Molecular, Instituto Superior Técnico, Universidade Técnica de Lisboa, Lisboa, Portugal

Received May 18, 2005; Revised Manuscript Received August 18, 2005

ABSTRACT: The HIV-1 gp41 envelope protein mediates the entry of the virus into the target cell by promoting membrane fusion. With a view toward possible new insights into the protein membrane alteration leading to the viral fusion mechanism, we have studied by infrared and fluorescence spectroscopies a fragment of 21 amino acids corresponding to the N-heptad repeat region of the gp41 ectodomain. Information on the structure of the peptide both in solution and in the presence of model membranes, its incorporation and location in the phospholipid bilayer, and the modulation of the phase behavior of the membrane has been gathered. Here we demonstrate that the peptide binds to and interacts with phospholipid model membranes, changing its conformation and inducing leakage of vesicle contents. These characteristics suggest that different specific regions of gp41 are capable of modifying the biophysical properties of phospholipid membranes and, therefore, might be essential for the assistance and enhancement of the viral and cell fusion process.

The human immunodeficiency virus (HIV)[1] is the causative agent of the acquired immunodeficiency syndrome, which acts by killing CD4 T-cells of the host organism (*1*−*3*). Membrane fusion, i.e., the attachment and the consequent fusion of viral and cellular membranes, is mediated by envelope glycoproteins located on the outer surface of the viral membrane: gp120, the surface protein that determines the viral tropism, and gp41, the transmembrane protein which is responsible for the membrane fusion process. gp41 must undergo a complex series of conformational changes so that fusion and mixing of the viral and cellular contents take place, apparently triggered by the attachment of gp120 to CD4 and chemokine receptors of the target cell (*4*). It is thought that gp41 catalyzes membrane fusion through the induction of transient nonlamellar structures at the point where both bilayers merge (*1*, *2*). The gp41 sequence is highly conserved and contains different functional regions within its ectodomain that are critical for membrane fusion, i.e., the fusion peptide, two heptad repeat regions, the Trp-rich pre-transmembrane domain, and the loop domain (*5*−*9*). These regions of the gp41 glycoprotein have the capabilities of binding and partitioning into the surface of phospholipid model membranes, change their conformation, and induce the formation of nonlamellar structures, indicating that these segments could play an essential role in the viral fusion process (*7*−*13*). Although much information has been gathered in recent years, we do not know yet the different processes and mechanism of membrane fusion.

Recently, we have investigated the binding and interaction of different segments of the gp41 glycoprotein with different types of model membranes, and the results obtained indicate that, depending on the specific phospholipid composition of the model membranes, they change their conformation upon binding to the membrane as well as they modulate the phospholipid behavior (refs *8* and *10* and unpublished experiments). Anionic lipids are integral components of biological membranes and are invariably present in substantial quantities, having specific functions in biological membranes (*14*, *15*). Much circumstantial evidence has accumulated suggesting that the electrostatic interactions between the anionic lipids headgroups and positively charged residues of proteins and peptides are crucial in the association of protein or peptides with membranes (*16*). In view of the potential importance of the membrane negative character, anionic phospholipids have been widely used as model

† This work was partly supported by Grants BMC2002-00158 (Ministerio de Ciencia y Tecnología, Spain) and LSHB-CT-2003-503480 (European Union project "Targeting Replication and Integration of HIV", TRIoH) to J.V. R.P. is a recipient of a predoctoral fellowship from the Ministerio de Educación, Cultura y Deporte, Spain.

* Corresponding author. Tel: +34 966 658 762. Fax: +34 966 658 758. E-mail: jvillalain@umh.es.

‡ Universidad "Miguel Hernández".

§ Universidad de Carabobo.

|| Universidade Técnica de Lisboa.

[1] Abbreviations: ANTS, 8-aminonaphthalene-1,3,6-trisulfonic acid; CHR, C-terminal heptad repeat; DMPA, 1,2-dimyristoyl-*sn*-glycerophosphatidic acid; DMPC, 1,2-dimyristoyl-*sn*-glycerophosphatidylcholine; $DMPC_d$, 1,2-dimyristoyl-d_{54}-*sn*-glycero-3-phosphocholine; DMPG, 1,2-dimyristoyl-*sn*-glycerophosphatidylglycerol; DPH, 1,6-diphenyl-1,3,5-hexatriene; DPX, *p*-xylenebis(pyridinium bromide); EPA, egg phosphatidic acid; EPC, egg phosphatidylcholine; EPG, egg phosphatidylglycerol; FP, fusion peptide; HIV, human immunodeficiency virus; LUV, large unilamellar vesicles; MLV, multilamellar vesicles; NBD-PE, *N*-(7-nitrobenz-2-oxa-1,3-diazol-4-yl)-1,2-dihexadecanoyl-*sn*-glycero-3-phosphoethanolamine; NHR, N-terminal heptad repeat; N-Rh-PE, Lissamine rhodamine B 1,2-dihexadecanoyl-*sn*-glycero-3-phosphoethanolamine; PG, phosphatidylglycerol; PTM, pre-transmembrane domain; SUV, small unilamellar vesicles; T_m, temperature of the gel-to-liquid crystalline phase transition; TM, transmembrane domain; TMA-DPH, 1-[4-(trimethylammonio)phenyl]-6-phenyl-1,3,5-hexatriene.

10.1021/bi050928+ CCC: $30.25
Published on Web 10/07/2005

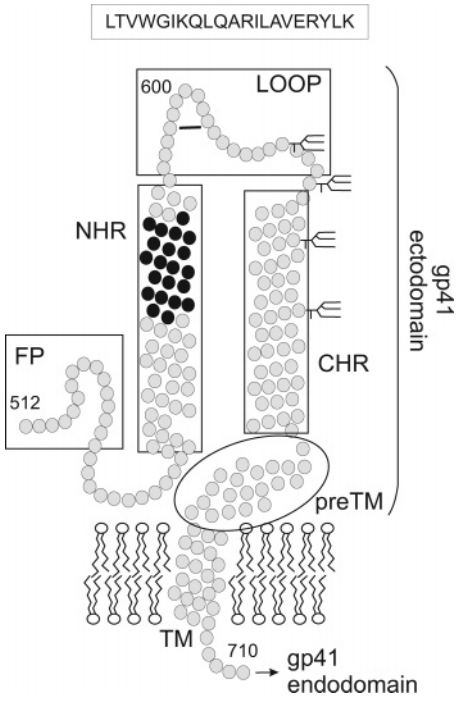

FIGURE 1: Updated model of the HIV_{HXB2} gp41 ectodomain showing the structural and functional regions as well as their relative lengths. The fusion peptide (FP), the loop, the NHR and CHR heptad repeats, the pre-transmembrane stretch (PTM), and the transmembrane (TM) domain have been drawn approximately to scale. The residue numbers correspond to their positions in gp160 of the HIV_{HXB2} strain, whereas the sequence and location of the gp41 fragment studied in this work are indicated.

systems for anionic domains. Viral membrane fusion continues to be an important topic of research since it serves as a model for cellular fusion events and it is a very good target for therapeutic intervention (*17*). In this sense, elucidating the nature of the interactions between negatively charged phospholipids and membrane proteins and peptides is important for the understanding of the structure and function of membrane proteins and to clarify the specific roles of these specific types of phospholipids in biological membranes. In this report we describe the effects of a peptide pertaining to the NHR region of the gp41 ectodomain, analogous to residues 568−588 of the HXB2 strain (see Figure 1), on the thermotropic phase behavior of phospholipid model membranes. The structural changes which take place in both the peptide and phospholipid molecules induced by the binding, specific interaction process, and its relationship to the membrane perturbation leading to gp41-mediated membrane fusion between the viral and host cell membranes are presented.

MATERIALS AND METHODS

Materials. The HIV envelope protein gp41 fragment (LTVWGIKQLQARILAVERYLK) corresponding to amino acids 568−588 from the HIV_{HXB2} strain was synthesized as a C-terminal amide on an automatic multiple synthesizer (Genemed Synthesis, San Francisco, CA). The peptide was purified by reverse-phase HPLC to better than 95% purity, and its composition and molecular mass were confirmed by amino acid analysis and mass spectroscopy. Since trifluoroacetate has a strong infrared absorbance at approximately 1673 cm^{-1}, which interferes with the characterization of the peptide amide I band (*18*), residual trifluoroacetic acid used both in the peptide synthesis and in the HPLC mobile phase was removed by several lyophilization/solubilization cycles in 10 mM HCl (*19*). 1,2-Dimyristoyl-*sn*-glycerophosphatidylcholine (DMPC), 1,2-dimyristoyl-d_{54}-*sn*-glycero-3-phosphocholine ($DMPC_d$), 1,2-dimyristoyl-*sn*-glycerophosphatidylglycerol (DMPG), 1,2-dimyristoyl-*sn*-glycerophosphatidic acid (DMPA), egg phosphatidylcholine (EPC), egg phosphatidylglycerol (EPG), and egg phosphatidic acid (EPA) were obtained from Avanti Polar Lipids (Birmingham, AL). Deuterium oxide (99.9% by atom), HEPES, Triton X-100, and EDTA were purchased from Sigma (St. Louis, MO), whereas Lissamine rhodamine B 1,2-dihexadecanoyl-*sn*-glycero-3-phosphoethanolamine (N-Rh-PE), *N*-(7-nitrobenz-2-oxa-1,3-diazol-4-yl)-1,2-dihexadecanoyl-*sn*-glycero-3-phosphoethanolamine (NBD-PE), 1,6-diphenyl-1,3,5-hexatriene (DPH), 1-[4-(trimethylammonio)phenyl]-6-phenyl-1,3,5-hexatriene (TMA-DPH), 8-aminonaphthalene-1,3,6-trisulfonic acid (ANTS), and *p*-xylenebis(pyridinium bromide) (DPX) were obtained from Molecular Probes (Eugene, OR). All other chemicals were commercial samples of the highest purity available (Sigma-Aldrich, Madrid, Spain). Water was twice distilled and deionized in a Millipore system (Millipore, Madrid, Spain).

Sample Preparation. For IR spectroscopy, aliquots containing the appropriate amount of lipid in chloroform/methanol (2:1 v/v) were placed in a test tube, the solvents removed by evaporation under a stream of O_2-free nitrogen, and, finally, traces of solvents were eliminated under vacuum in the dark for more than 3 h. The lipid films were resuspended in 200 μL of 20 mM HEPES, 50 mM NaCl, and 0.1 mM EDTA, pH 7.4, in either D_2O or H_2O and incubated at 10 °C above the T_m with intermittent vortexing for 45 min to hydrate the samples and obtain multilamellar vesicles (MLV). When required, peptide in buffer was added to the lipid films to obtain a final lipid-to-peptide mole ratio of 30:1. The samples were frozen and thawed five times to ensure complete homogenization and maximization of peptide/lipid contacts with occasional vortexing. Finally, the suspensions were centrifuged at 15000 rpm at 25 °C for 10 min to remove the peptide that was not bound to the membrane. The pellet was incubated for 45 min at 10 °C above the T_m of the lipidic mixture and used for the measurements, except for metastability time-resolved experiments where some samples were incubated at 4 °C.

For fluorescence anisotropy experiments, MLV samples were prepared as above, and aliquots of stock solutions of either DPH or TMA-DPH in *N*,*N*′-dimethylformamide (2×10^{-4} M) were directly added into the lipid dispersion to obtain a probe-to-lipid molar ratio of 1:750. To incorporate the probes, the samples were incubated at 55 °C for 60 min in the case of DPH and 15 min in the case of TMA-DPH. In all cases the peptide-to-lipid ratio was 30:1. For binding fluorescence studies, small unilamellar vesicles (SUV) were used (*20*) in order to have lower scattering effects. First, MLV were obtained as described above using H_2O buffer, except that no peptide was present. The lipid suspension was frozen and thawed five times to ensure complete hydration and mixing of the phospholipid, and the resulting multilamellar suspension was sonicated with a Branson 250 sonifier (40 W) equipped with a microtip until the suspension became completely transparent. Every 30 s, the samples were

cooled for 90 s in ice to prevent overheating of the solution. The titanium particles released from the tip were removed by centrifugation at 15000 rpm at room temperature for 15 min. The membrane incorporation studies were performed by adding small volumes of this suspension to a solution containing a known amount of peptide (2.9 μM), followed by an incubation at 30 °C for 15 min before measurements. Large unilamellar vesicle (LUV) liposomes were used to study vesicle aggregation, lipid mixing, and leakage, and they were prepared by the extrusion method (*21*) using polycarbonate filters with a pore size of 0.1 μm (Nuclepore, Pleasanton, CA). The buffer used for preparing LUV liposomes for assays of vesicle leakage contained in addition 25 mM ANTS and 90 mM DPX. Nonencapsulated fluorescent probes were separated from the vesicle suspension through a Sephadex G-75 filtration column (Pharmacia, Uppsala, Sweden) eluted at room temperature with 10 mM HEPES, 130 mM NaCl, and 0.1 mM EDTA, pH 7.4, buffer. For some experiments, unsaturated phospholipids instead of saturated ones were used because of the great variability in the basal fluorescence using the last ones.

The phospholipid and peptide concentrations were measured by methods described previously (*22*, *23*).

Infrared Spectroscopy. Approximately 25 μL of a pelleted sample in either D_2O or H_2O was placed between two CaF_2 windows separated by either 50 μm (D_2O) or 6 μm (H_2O) thick Teflon spacers in a liquid demountable cell (Harrick, Ossining, NY). The spectra were obtained in a Bruker IFS55 spectrometer using a deuterated triglycine sulfate detector. Each spectrum was obtained by collecting 200 interferograms with a nominal resolution of 2 cm^{-1}, transformed using triangular apodization, and to average background spectra between sample spectra over the same time period, a sample shuttle accessory was used to obtain sample and background spectra. The spectrometer was continuously purged with dry air at a dew point of −40 °C in order to remove atmospheric water vapor from the bands of interest. All samples were equilibrated at the lowest temperature for 20 min before acquisition. An external bath circulator, connected to the infrared spectrometer, controlled the sample temperature. For temperature studies, samples were scanned using 2 °C intervals and a 2 min delay between each consecutive scan. Subtraction of buffer spectra taken at the same temperature as the samples was performed interactively using either GRAMS/32 or Spectra-Calc (Galactic Industries, Salem, MA) as described previously (*10*, *24*). Frequencies at the center of gravity, when necessary, were measured by taking the top 10 points of each specific band and fitted to a Gaussian band. Band-narrowing strategies were applied in order to resolve the component bands in the amide I′ region. Second-derivative spectra were calculated over a 15 data point range. Fourier self-deconvolution (*25*) of the subtracted spectra was carried out using a Lorentzian shape and a triangular apodization with a resolution enhancement parameter, *K*, of 2.2, which is lower than log(signal/noise) (*26*) and a full width at half-height of 18 cm^{-1}. These parameters assume that the spectra were not over-deconvolved as was evidenced by the absence of negative side lobes. Protein secondary structure elements were quantified from curve-fitting analysis by band decomposition of the original amide I′ band after spectral smoothing using the same software stated above (*24*, *27*). Briefly, for each component, three parameters were considered: band position, band height, and band width. The number and position of component bands were obtained through deconvolution, and in decomposing the amide I′ band, Gaussian components were used. The curve-fitting procedure was accomplished in two steps: in the first one, band position was fixed, allowing width and heights to approach final values, and in the second one, band positions were left to change. When necessary, these two steps were repeated. Band decomposition was performed using SpectraCalc (Galactic Industries, Salem, MA). The fitting result was evaluated visually by overlapping the reconstituted overall curve on the original spectrum and by examining the residual obtained by subtracting the fitting from the original curve. The procedure gave differences of less than 2% in band areas after the artificial spectra were submitted to the curve-fitting procedure. The frequency positions of the band centers were independently evaluated by second derivative procedures, being always very close to the positions found by deconvolution.

Fluorescence Spectroscopy. Steady-state fluorescence measurements were carried out using a SLM 8000C spectrofluorometer with a 400 W Xe lamp, double emission monochromator, and Glan-Thompson polarizers. Correction of excitation spectra was performed using a rhodamine B solution and a standard lamp. Typical spectral bandwidths were 4 nm for excitation and 2 nm for emission. All fluorescence studies were carried using 5 mm × 5 mm quartz cuvettes. The excitation and emission wavelengths were 360/362 and 425/450 nm when observing the DPH and TMA-DPH fluorescence, respectively. All of the data were corrected for background intensities and progressive dilution. Emission spectra were not corrected for the photomultiplier wavelength dependence, since no absolute quantum yield values were needed. Fluorescence anisotropies and leakage were determined as described previously (*10*). To monitor membrane fusion, two types of SUVs were prepared: one set contained 0.6 mol % of the fluorescent lipid NBD-PE and 0.6 mol % of the quenching lipid N-Rh-PE, whereas the other one contained unlabeled lipids (*28*). Fluorescently labeled and unlabeled vesicles were mixed in a 1:9 ratio. After addition of peptides, lipid mixing between labeled and unlabeled vesicles caused dilution of the labeled lipids in the membrane volume, with a resulting increase of fluorescence. Partition constants K_p were determined by using the equation:

$$r = \frac{K_p Y r_L + D r_W}{D + K_p Y} \quad (1)$$

where r_L and r_W are the anisotropies in the lipidic and aqueous phases, respectively, $Y = \Phi_L/\Phi_W$, $D = (1/\gamma_L) - 1$, L is the lipid concentration, γ is the lipid molar volume, and Φ_L and Φ_W are the fluorescence quantum yields in both phases.

The instrumentation for fluorescence decay measurements by the single photon-timing technique with pulsed laser excitation was described previously (*29*). For excitation of the sample at a wavelength of 295 nm, a laser of rhodamine 6G (Coherent 701-2), synchronously pumped by a mode-locked Ar^+ laser (514.5 nm; Coherent Innova 400-10), was used, and detection was carried out with a Hamamatsu R-2809 MCP photomultiplier. Emission at 350 nm was

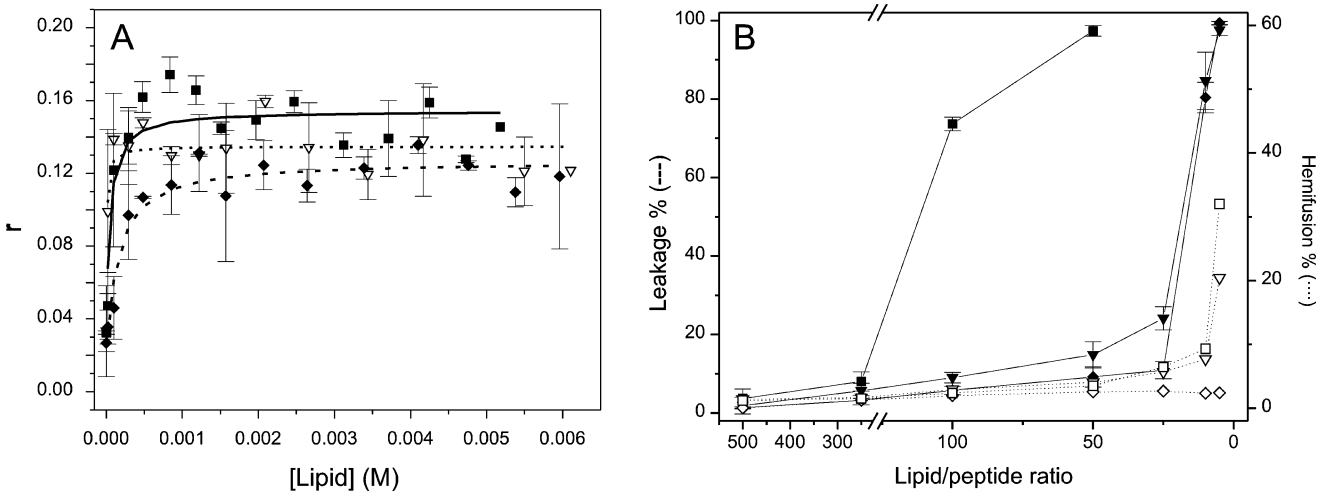

FIGURE 2: (A) Fluorescence anisotropy of the gp41 fragment in the presence of increasing concentrations of SUV composed of EPG (■), EPA (▽), and EPC (◆) and (B) effect of the gp41 fragment on leakage data at 25 °C for LUV contents (—, filled symbols) and phospholipid mixing (···, open symbols) for different lipid compositions and different lipid-to-peptide molar ratios: EPG (■, □), EPA (▼, ▽), and EPC (◆, ◇). See text for details.

detected at the magic angle relative to the vertically polarized excitation beam. The number of counts on the peak channel was 20000, and the number of channels per curve used for the analysis was 1024, with a time scale of 20 or 22 ps per channel at 15 °C and room temperature and 15 or 11 ps per channel at 50 °C. Data analysis was carried out using a nonlinear, least-squares iterative convolution method based on the Marquardt algorithm. Fitting goodness was judged from the global chi-square value (χ^2), weighted residuals, and autocorrelation plot. The average lifetime of a fluorophore, $\bar{\tau}$, is

$$\bar{\tau} = \sum_i \alpha_i \tau_i^2 / \sum_i \alpha_i \tau_i \qquad (2)$$

where τ_i is the fluorescence lifetime of component i and α_i is the respective normalized preexponential factor, which is proportional to the concentration of the component. To obtain partition coefficients, the lifetime-weighted quantum yield $\langle\tau\rangle$ is in turn defined by

$$\langle\tau\rangle = \sum_i \alpha_i \tau_i \qquad (3)$$

RESULTS

Peptide Membrane Binding and Interaction. The ability of the gp41$^{568-588}$ peptide to interact with membranes was determined from fluorescence anisotropy values of its Trp residue in the presence of phospholipid model membranes at different lipid-to-peptide ratios (Figure 2A). The anisotropy values of the gp41$^{568-588}$ peptide increased upon increasing the lipid-to-peptide ratio, indicating a significant motional restriction of the Trp moiety of the peptide (*30*). The change in the anisotropy values of the Trp fluorescence of the peptide allowed us to obtain its partition coefficient, K_p. Considering a γ value of 0.519 M^{-1} (*31*), K_p values of $(4 \pm 1) \times 10^3$ for EPC, $(7.9 \pm 3.9) \times 10^4$ for EPA, and $(1.25 \pm 0.6) \times 10^4$ for EPG were obtained, indicating that the peptide was bound to the membrane surface with high affinity. Similar K_p values have been found for other peptides pertaining to the gp41 protein in the presence of negatively charged phospholipid-containing model membranes (*8*, *10*, *31*). These results were further corroborated by the change in the emission frequency maximum of Trp. In solution the peptide had an absorbance maximum at 295 nm and an emission maximum at 353 nm when excited at the absorbance maximum, indicating that the Trp residue of the peptide is located in a hydrophilic environment. In the presence of increasing concentrations of either EPC, EPA, or EPG, the emission maximum of the Trp did change from 353 to 335 nm, implying that Trp sensed a low-polarity environment upon interaction with the membrane. From the fitting procedure of eq 1 used for K_p determination, the anisotropies (r_L) of the peptide in the presence of EPA, EPC, and EPG, respectively, were 0.135, 0.127, and 0.150, pointing out to a significant peptide immobilization when in the membrane.

To further explore the interaction of the gp41$^{568-588}$ peptide with phospholipid model membranes, we studied the effect of the peptide on the release of encapsulated fluorophores. Figure 2B shows the results obtained with different liposome compositions, namely, EPC, EPA, and EPG. In the presence of EPG there were significant leakage values, since at a lipid-to-peptide ratio of 100:1 a leakage of about 75% was observed, but lower values were found in the presence of EPC and EPA. We also studied phospholipid mixing, where we found significant values for EPG- and EPA-containing liposomes at low lipid-to-peptide ratios but no phospholipid mixing for EPC-containing liposomes (Figure 2B). In addition to a lower value of K_p for EPC, curvature degree, i.e., capability to obtain nonlamellar phases, is greater for EPG and EPA than for EPC, and this might also explain why we have observed lipid mixing in EPG- and EPA-containing liposomes. The peptide also induced liposome aggregation (results not shown), as observed by the increase in light scattering for liposomes composed of either EPG or EPA and also EPC, but only at very low ratios of lipid to peptide, i.e., 5:1.

The effect of the gp41 peptide on the structural and thermotropic properties of phospholipid membranes was further investigated by measuring the steady-state fluorescence anisotropy of the fluorescent probes DPH and TMA-DPH incorporated into DMPC, DMPG, and DMPA membranes as a function of temperature. The gp41$^{568-588}$ peptide

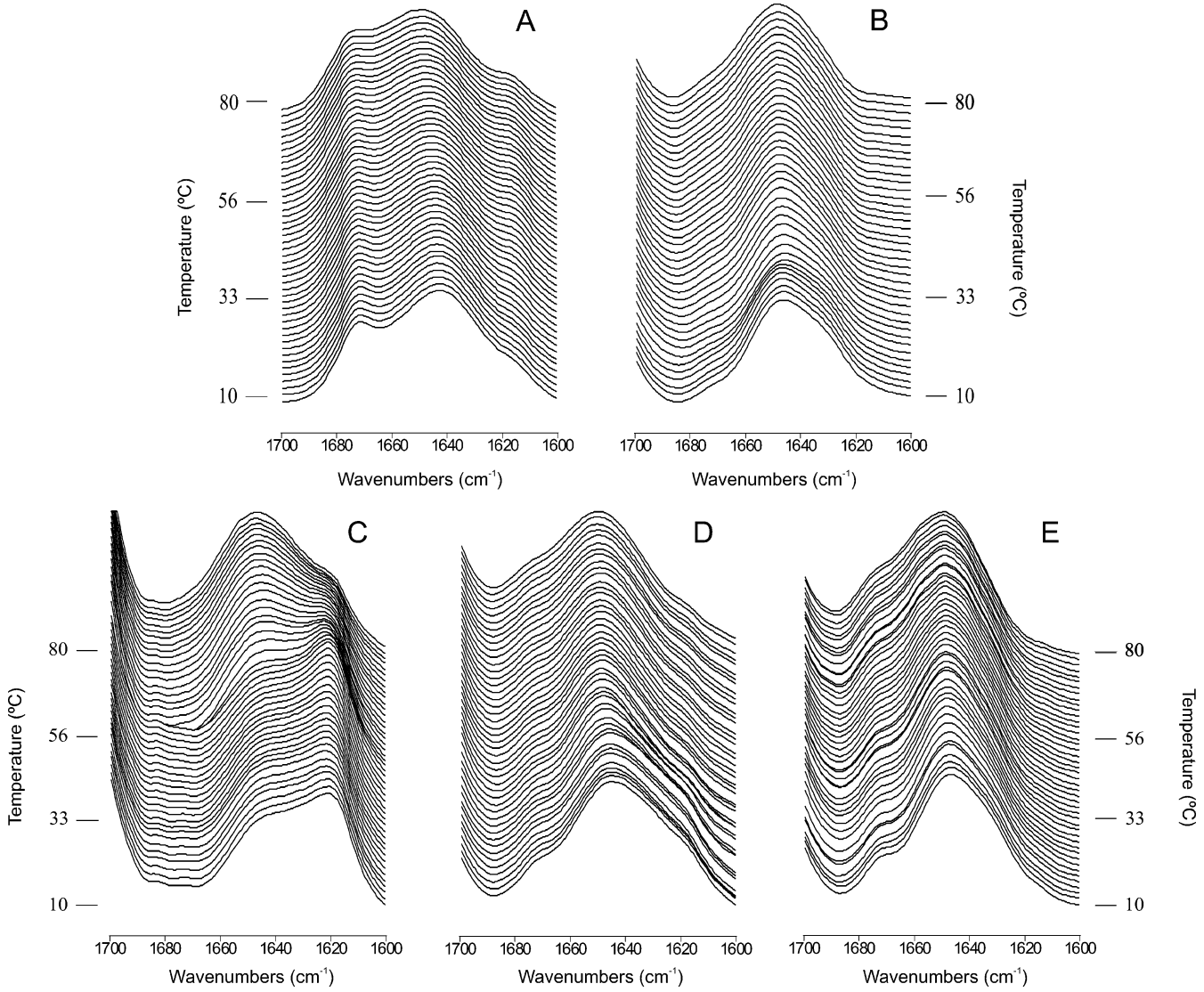

FIGURE 3: Stacked infrared spectra in the amide I′ region of the gp41$^{568-588}$ peptide in solution at a concentration of 3 mM (A) and in the presence of DMPG (B), DMPA (C), DMPC$_d$/DMPA at a molar ratio of 2:1 (D), and DMPC$_d$/DMPG at a molar ratio of 2:1 (E) at different temperatures as indicated. The phospholipid-to-peptide molar ratio was 30:1.

did not affect significantly the anisotropy of both probes for DMPC and DMPA both below and above the T_m of the phospholipids, indicating that the peptide was localized at the membrane surface (not shown). However, it decreased the cooperativity of the transition in the case of DMPG, increasing slightly the anisotropy above the gel-to-liquid crystalline phase transition of the phospholipid for both probes (not shown for briefness), indicating that the gp41$^{568-588}$ peptide fragment was inserted, although slightly, into the DMPG membrane palisade (*8*). It should be stressed that no quenching of the probes by the peptide was observed in this concentration range. In this way, this variation of anisotropy cannot be ascribed to a shorter probe lifetime.

Secondary Structure of the gp41 Peptide in the Presence of Phospholipid Model Membranes. The infrared spectra of the amide I′ region of the fully hydrated gp41$^{568-588}$ peptide in D_2O buffer at different temperatures and at pH 7.4 are shown in Figure 3A. The spectra were formed by different underlying components that gave place to a broad and asymmetric amide I′ band with a frequency maximum of about 1643 and 1647 cm^{-1} at 20 and 77 °C, respectively. The amide I′ envelope was also characterized by two smaller broad bands located at approximately 1676 and 1617 cm^{-1}. Protein denaturation is characterized in D_2O medium by the appearance of two sharp bands at approximately 1685 and 1620 cm^{-1}, due to extended β-strands with strong intermolecular interactions (*32*). These bands were not visible in the whole range of temperatures studied so that if aggregation occurred, it was only to a low extent. The spectra showed a small change in the maximum of the bands as the temperature was increased. An increase in the bandwidth at half-height of the bands at high temperatures compared to those at low temperatures was also visible (Figures 3A), indicating that, in solution, the peptide possesses a high degree of conformational stability.

The infrared spectra in the amide I′ region of the gp41$^{568-588}$ peptide in the presence of DMPG, DMPA, DMPC$_d$/DMPG, and DMPC$_d$/DMPA at molar ratios of 2:1 and at a phospholipid-to-peptide molar ratio of 30:1 are shown in panels B−E of Figure 3, respectively. The broad band which appeared at approximately 1676 cm^{-1} in the amide I′ region of the peptide in solution decreased in intensity in the presence of all phospholipid model membrane systems studied; i.e., the proportion of β-turn structure

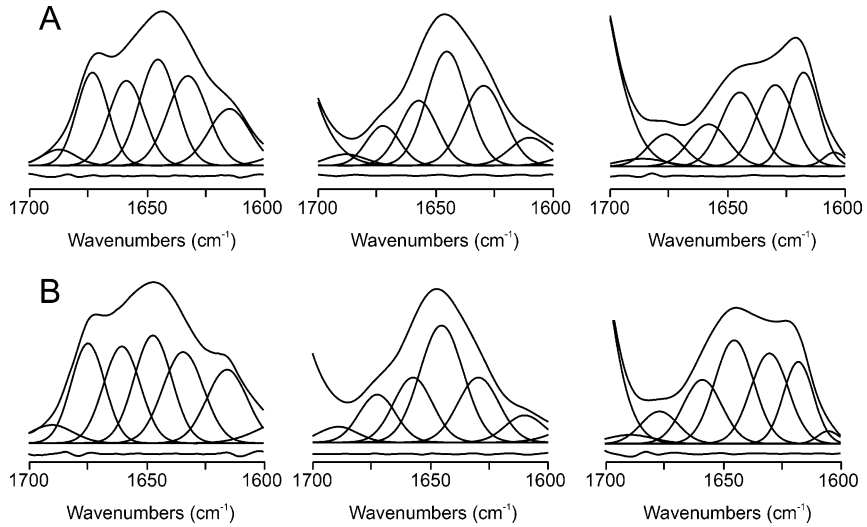

FIGURE 4: Amide I′ band decomposition of the gp41$^{568-588}$ peptide spectra in solution and in the presence of DMPG and DMPA (from left to right). The spectra were taken at 10 °C below (A) and 10 °C above (B) the phospholipid T_m, except for the peptide in solution where the temperature values were 15 and 60 °C, respectively. The component bands, the original envelope, and the difference between the fitted curve and the original spectrum are shown. See text for details.

decreased (*32*); therefore, the secondary structure of the bound peptide is different from that found in solution. What is indeed significant is that, as shown in Figure 3C, the amide I′ region of the gp41$^{568-588}$ peptide in the presence of DMPA taken at temperatures above and below the main phase transition temperature of the phospholipid was different: whereas at low temperatures the maximum of the amide I′ envelope appeared at about 1621 cm^{-1}, at high temperatures the maximum of the band was 1643 cm^{-1}, in this last case similarly to the one in solution (compare panels A and C of Figure 3). Outstandingly, the change in frequency took place at the same temperature as the phase transition T_m of DMPA took place as well as it was observed at different lipid-to-peptide ratios (not shown for briefness). These data suggest that the gp41$^{568-588}$ peptide has a different and distinct conformation in the presence of different phospholipid phases (vide infra). This is in contrast with the results found for the peptide in solution, where no significant differences were found at all temperatures studied, even at the highest one tested (Figure 3A).

To observe the underlying components of the broad amide I′ band, we have applied self-deconvolution and derivative methods to the original envelope (*24*, *32*). For the peptide in solution we have identified different component bands at frequencies of about 1687, 1672, 1657, 1645, 1632, and 1617 cm^{-1} at 15 and 60 °C (panels A and B of Figure 4, respectively). The results of the decomposition of the amide I′ of the gp41 fragment in the presence of two different model membrane systems, DMPG and DMPA, are also shown in Figure 4; it is also possible to distinguish different component bands having similar frequencies as those found for the peptide in solution, i.e., bands at about 1686, 1672, 1658, 1645, 1632, and 1617 cm^{-1}. To assign the component bands to specific structural features and estimate the percentage of each component, we have decomposed the amide I′ infrared band as described in Materials and Methods and compared them to literature values (*32*). Bands appearing at about 1637−1630 cm^{-1} are characteristic of β-sheet structures, whereas component bands at about 1670 and 1690 cm^{-1} are assigned to β-turns. Bands located at about 1657−1655 cm^{-1} are usually observed for the α-helix in D_2O solution, and bands appearing at about 1646−1641 cm^{-1} are assigned in D_2O to both unordered structures and α-helices. Bands appearing at about 1622 cm^{-1} have also been assigned to extended β-strands with strong intermolecular interactions, i.e., aggregated structures. Bands below 1620 cm^{-1} are outside the range of frequencies usually observed for the secondary structure elements of proteins. The most significant difference between the peptide amide I′ band in solution and in the presence of DMPG is the increase in the relative intensity of the band appearing at 1645 cm^{-1}, as well as the decrease in the relative intensity of the bands assigned to β-turns, both at low and high temperatures (Table 1). However, it should be noted that it might be possible that the component band pertaining to β-turn structures might be altered by the change in the intensity of the bands pertaining to aggregated structures (Figure 4). Most interesting and significant is the change in the relative intensities for the component bands of the peptide in the presence of DMPA-containing vesicles. At low temperatures, i.e., below the phase transition of DMPA, the bands related to β-sheet structures were of higher intensity than those related to random structures; however, at high temperatures the contrary was true; i.e., the relative intensity of the bands related to β-sheet structures was of lower intensity than those related to random structures (compare panels A and B of Figure 4). Moreover, if we compare the relative intensity of the band

Table 1: Secondary Structure Content of the gp41 Peptide Fragment As Determined by Infrared Spectroscopy[a]

	peptide	% random (1641−1649 cm^{-1})	% β-sheet (1625−1640 cm^{-1})	% α-helix/3_{10}-helix (∼1650−1670 cm^{-1})	% β-turn (1670−1690 cm^{-1})
15 °C	in solution	28	26	22	24
T_m − 10 °C	+DMPG	38	27	20	15
	+DMPA	31	34	18	17
60 °C	in solution	27	24	23	26
T_m + 10 °C	+DMPG	40	22	20	19
	+DMPA	34	30	21	14

[a] The values are rounded off to the nearest integer.

Table 2: Lifetimes τ_i, Normalized Amplitudes α_i, and Fluorescence Mean Lifetimes (Eqs 2 and 3) of the Trp Residue of the gp41$^{568-588}$ Peptide in the Presence of All Phospholipid Model Membranes Assayed in This Work

	temp (°C)	α_1	τ_1	α_2	τ_2	α_3	τ_3	$\langle\tau\rangle$	χ^2
gp41$^{568-588}$	15	0.32	1.08	0.50	3.72	0.19	6.57	3.42	1.53
peptide	25	0.29	0.33	0.41	2.12	0.30	5.13	2.51	1.26
	50	0.28	0.32	0.61	1.52	0.11	4.34	1.50	1.07
+DMPC	15	0.26	0.40	0.39	2.46	0.35	5.80	3.08	1.35
	50	0.32	0.48	0.56	1.83	0.12	5.84	1.88	1.13
+DMPG	15	0.28	0.61	0.49	2.65	0.23	6.47	2.96	1.27
	50	0.35	0.51	0.52	1.94	0.13	5.62	1.91	1.17
	4	0.30	0.63	0.50	2.59	0.21	6.53	2.85	1.18
+DMPA	15	0.56	0.29	0.32	1.24	0.12	4.67	1.10	1.27
	50	0.41	0.30	0.45	1.24	0.13	3.78	1.19	1.34
+EPC	25	0.34	0.51	0.52	2.90	0.14	8.25	2.84	1.14
+EPG	25	0.33	0.44	0.46	2.28	0.20	6.26	2.48	1.30
+EPA	25	0.39	0.62	0.51	2.72	0.10	8.97	2.54	1.30

appearing at approximately 1617 cm^{-1} in the presence of DMPA, its intensity is much higher than in the presence of the other phospholipid membranes studied and comparable to the relative intensity this band has in solution (Table 1). It should also be noted that the relative intensity of the band pertaining to random structures for the peptide in the presence of DMPG had always higher intensity than in the presence of DMPA and the contrary was found for the component band of the peptide pertaining to β-sheet structures. Even more remarkable is the change on the amide I′ envelope which takes place at the phase transition of DMPA, implying a change in conformation occurring at the same time the phospholipid changes from the gel lamellar phase to the liquid crystalline phase.

We have also analyzed the fluorescence decay of the Trp residue of the peptide both in solution and in the presence of model membranes, and this was better described by three exponentials. As observed in Table 2, in the presence of unsaturated phospholipids and in the presence of DMPC and DMPG there is not a significant variation in the lifetimes with respect to the values found for the peptide in solution. It should be stressed that these values are not biased by the fraction of peptide in solution. Since the partition coefficients are known, this eventual effect can be taken into account such as described in a previous work (eq 6 in ref *31*). No significant variation of the corrected values, as compared to the experimental ones, was obtained. However, a significant decrease in the values was found for the peptide in the presence of DMPA. This decrease might be due to a dynamic self-quenching as a consequence of the peptide aggregation which takes place in the presence of DMPA and in the gel state (as found by infrared spectroscopy, vide supra). The fact that this decrease was not found in the presence of EPA might be due to the fact that this unsaturated phospholipid does not present a phase transition in the temperature range studied; i.e., it is not in the gel state. In this way and assuming a similar K_p for this lipid, the peptide in EPA would be more randomly distributed, and not segregated, e.g., to gel line defects.

Modulation of Phospholipid Phase Behavior. Infrared spectroscopy has proved to be well suited to detect changes in both the structure and conformation of proteins and phospholipids in membranes, and in addition, variations in hydration, hydrogen bonding been and polarity at specific sites of the bilayer molecules can be discerned (*32*). Although it has been shown that the incorporation of transmembrane peptides in the phospholipid palisade of the membrane can affect not only the phospholipid chain order but also interchain coupling (*33*), a shift in the frequency of the CH_2 symmetric stretching band is a reliable index of the phase behavior of phospholipid dispersions (*34*). The temperature dependence of the CH_2 symmetric frequency of pure DMPG is shown in Figure 5A, where a highly cooperative change, corresponding to the gel-to-liquid crystalline phase transition, T_m, of the phospholipid, is observed at approximately 23 °C. In the presence of the gp41$^{568-588}$ peptide, the cooperativity of the gel-to-liquid crystalline phase transition of DMPG was significantly reduced, the phospholipid transition beginning at approximately 19 °C and finishing at approximately 35 °C. Significantly, the broad phase transition seems to be composed of two overlapped transitions occurring at about 21−23 and 32−34 °C (Figure 5A). However, no changes in the CH_2 symmetric frequency were observed below and above the T_m when compared with the pure phospholipid. It should be recalled that the amide I′ band envelope of the peptide, although different from that found for the peptide in solution, did not present any change at all temperatures in the presence of DMPG.

The temperature dependence of the CH_2 symmetric frequency of pure DMPA is shown in Figure 5B, where a highly cooperative change at approximately 47 °C corresponding to the gel-to-liquid crystalline phase transition, T_m, of the phospholipid is observed. In the presence of the gp41$^{568-588}$ peptide there was no change in the cooperativity of the phospholipid transition, but differing from what was observed previously for DMPG, the frequency of the CH_2 symmetric frequency in the presence of the peptide was decreased at all temperatures, indicating that the proportion of *trans* isomers was higher in the presence of the peptide than in the pure phospholipid. The amide I′ envelope of the peptide in the presence of DMPA was different above and below the T_m of the phospholipid (Figure 5B), indicating, as noted above, a change in the conformation of the peptide concomitant with the phase transition of DMPA.

We have also studied the effect of the peptide in phospholipid binary mixtures where the acyl chains of one phospholipid were perdeuterated ($DMPC_d$) and the other, the negatively charged one, was not, so that it is possible to detect independent changes in each phospholipid type. The CH_2 and CD_2 stretching frequencies of DMPG and $DMPC_d$ in the binary mixture, $DMPC_d$/DMPG, are shown in panels C and D of Figure 5, respectively. A single cooperative transition was observed for the pure binary mixture with mean T_m values of 23−24 °C, similarly to what has been found previously (*10*). The presence of the gp41$^{568-588}$ peptide induced a small change in the cooperativity of the transition for both types of lipids but no significant change in either the CD_2 stretching frequency of $DMPC_d$ or the CH_2 stretching frequency of DMPG (Figure 5C,D). The CH_2 and CD_2 stretching frequencies of DMPA and $DMPC_d$ in the binary mixture, $DMPC_d$/DMPA, are shown in panels E and F of Figure 5, respectively, where a single transition at about 34−35 °C was observed (*10*). The presence of the gp41$^{568-588}$ peptide induced a slight increase in the T_m values of DMPA and a decrease in the frequency below the T_m of the phospholipid (Figure 5E). In the case of $DMPC_d$, the

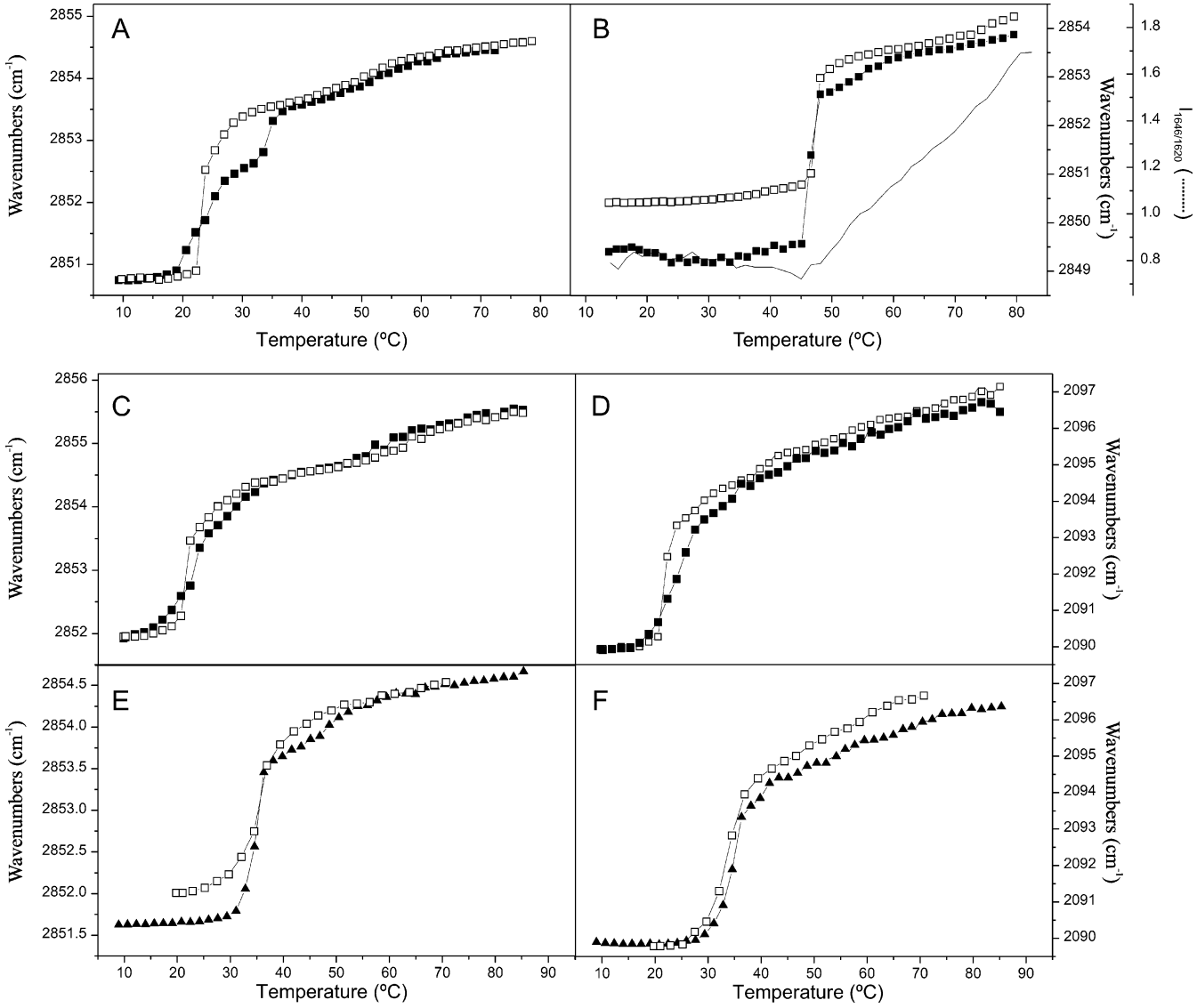

FIGURE 5: Temperature dependence of the CH_2 symmetric stretching band frequency of DMPG (A) and DMPA (B) in the absence (□) and in the presence (■) of the gp41$^{568-588}$ peptide at a phospholipid-to-peptide ratio of 30:1. The dotted line in (B) represents the 1646/1620 cm^{-1} band intensity ratio of the amide I′ band of the peptide in the presence of DMPA. Temperature dependence of the CH_2 symmetric stretching (C, E) and CD_2 symmetric stretching (D, F) band frequency of equimolar mixtures of $DMPC_d$/DMPG (C, D) and $DMPC_d$/DMPA (E, F) in the absence (□) and in the presence (■) of the gp41$^{568-588}$ peptide at a phospholipid-to-peptide ratio of 30:1.

presence of the peptide induced a slight increase in the T_m values of the phospholipid, concomitantly with a decrease in the CD_2 stretching frequency above the T_m (Figure 5F).

To better characterize the phases of both DMPA and DMPG, we have also examined the temperature dependence of the stretching vibration bands arising from the C═O ester of the phospholipids. It is generally accepted that the *sn*-1 and *sn*-2 groups of diacylphospholipids may be found in lipid vesicles in hydrated and dehydrated states, the proportion of hydrated and dehydrated groups depending on the physical state of the phospholipid bilayer (*35*). Pure DMPA showed a broad C═O carbonyl band (see Figure 6A) which presented, after deconvolution, two components at 1742 and 1727 cm^{-1} (not shown for briefness) attributed to dehydrated and hydrated C═O groups, respectively; the frequencies of these two components were not affected by temperature, but their relative intensities changed as reported for other phospholipids (*34*). Whereas below the phase transition the 1742 cm^{-1} component had a higher intensity than the 1727 cm^{-1} component, at temperatures above the phase transition just the opposite was observed. The C═O stretching region of DMPA in the presence of the gp41$^{568-588}$ peptide is shown in Figure 6B. The behavior of the C═O stretching band of DMPA in the presence of the peptide was similar to that found for the pure phospholipid, although an increase in half-bandwidth could be observed (the half-bandwidth of the C═O band of DMPA was about 35 and 38 cm^{-1} below and above the T_m of the phospholipid whereas in the presence of the peptide the half-bandwidth was 46 and 43 cm^{-1}, respectively). The frequency at the maximum of the C═O vibration band for both pure DMPA and DMPA in the presence of the gp41$^{568-588}$ peptide displayed a large cooperative transition corresponding to the gel-to-liquid crystalline phase transition of the phospholipid (Figure 6E), presenting a similar behavior to what was found for the CH_2 stretching frequencies (see Figures 5B and 6E).

In the case of DMPG, the pure phospholipid showed a broad C═O carbonyl band (see Figure 6C) which presented, after deconvolution, two components at 1742 and 1727 cm^{-1} (not shown for briefness). Similarly to what was found for

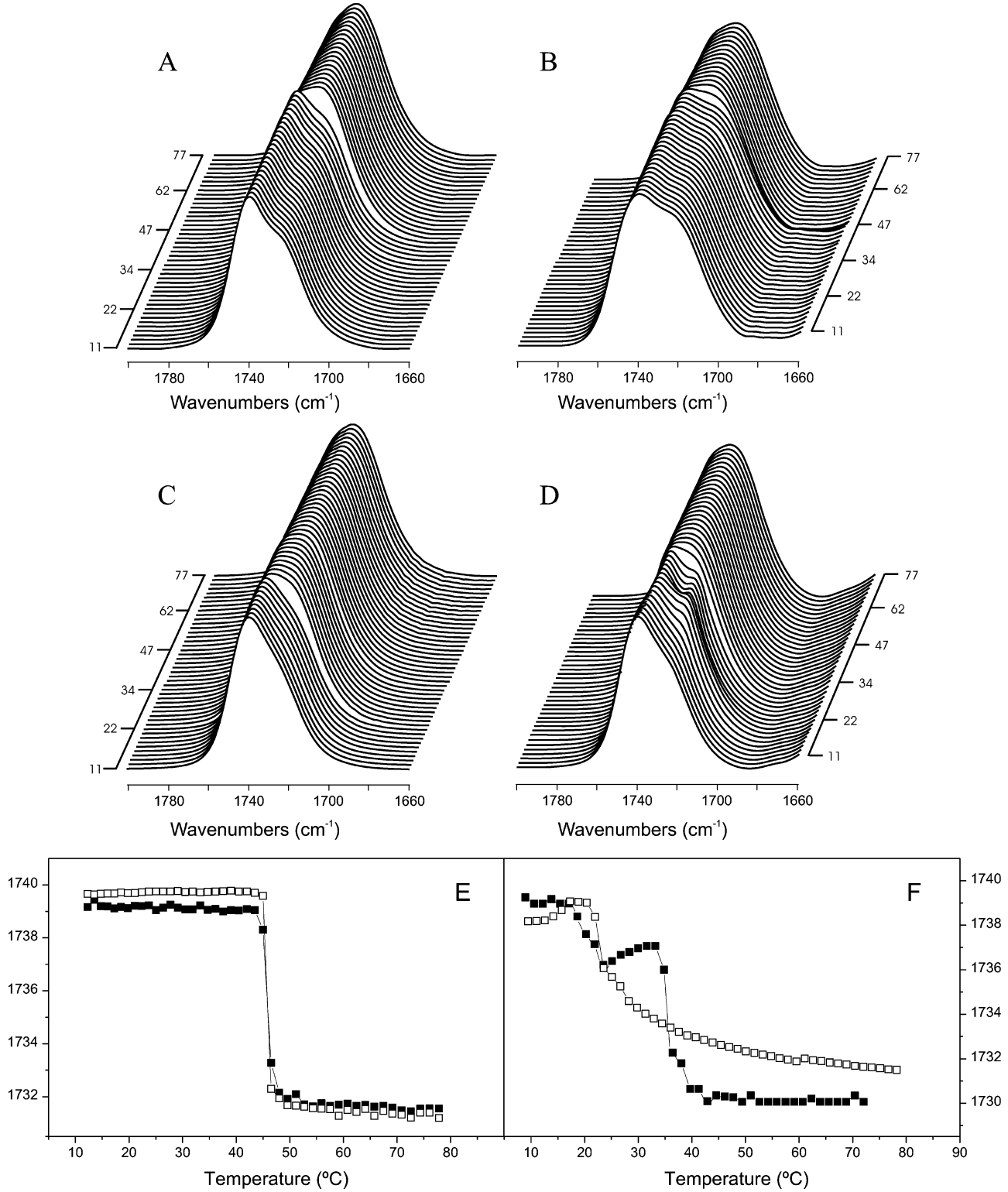

FIGURE 6: Stacked infrared spectra of the C═O stretching band of DMPA (A, B) and DMPG (C, D) in the absence (A, C) and in the presence (B, D) of the gp41$^{568-588}$ peptide at a phospholipid-to-peptide molar ratio of 30:1, recorded at regular intervals of temperature as indicated. The temperature dependence of the C═O maximum band frequency of DMPA and DMPG is indicated in (E) and (F), respectively, both in the absence (□) and in the presence (■) of the gp41$^{568-588}$ peptide at a phospholipid-to-peptide molar ratio of 30:1.

DMPA (vide supra), the 1742 cm^{-1} component had a higher intensity than the 1727 cm^{-1} component below the phase transition, whereas the opposite was observed above the phase transition. The frequency at the maximum of the C═O vibration band for pure DMPG can be observed in Figure 6F, where a slight increase in frequency corresponding to the pretransition of the pure phospholipid is observed at approximately 15 °C and a decrease of the frequency at about 23 °C, which corresponds to the main gel-to-liquid crystalline phase transition of the pure phospholipid. The C═O stretching region of DMPG at different temperatures and in the presence of the gp41$^{568-588}$ peptide is shown in Figure 6D. In this case, the behavior of the C═O stretching band of DMPG in the presence of the peptide is significantly different

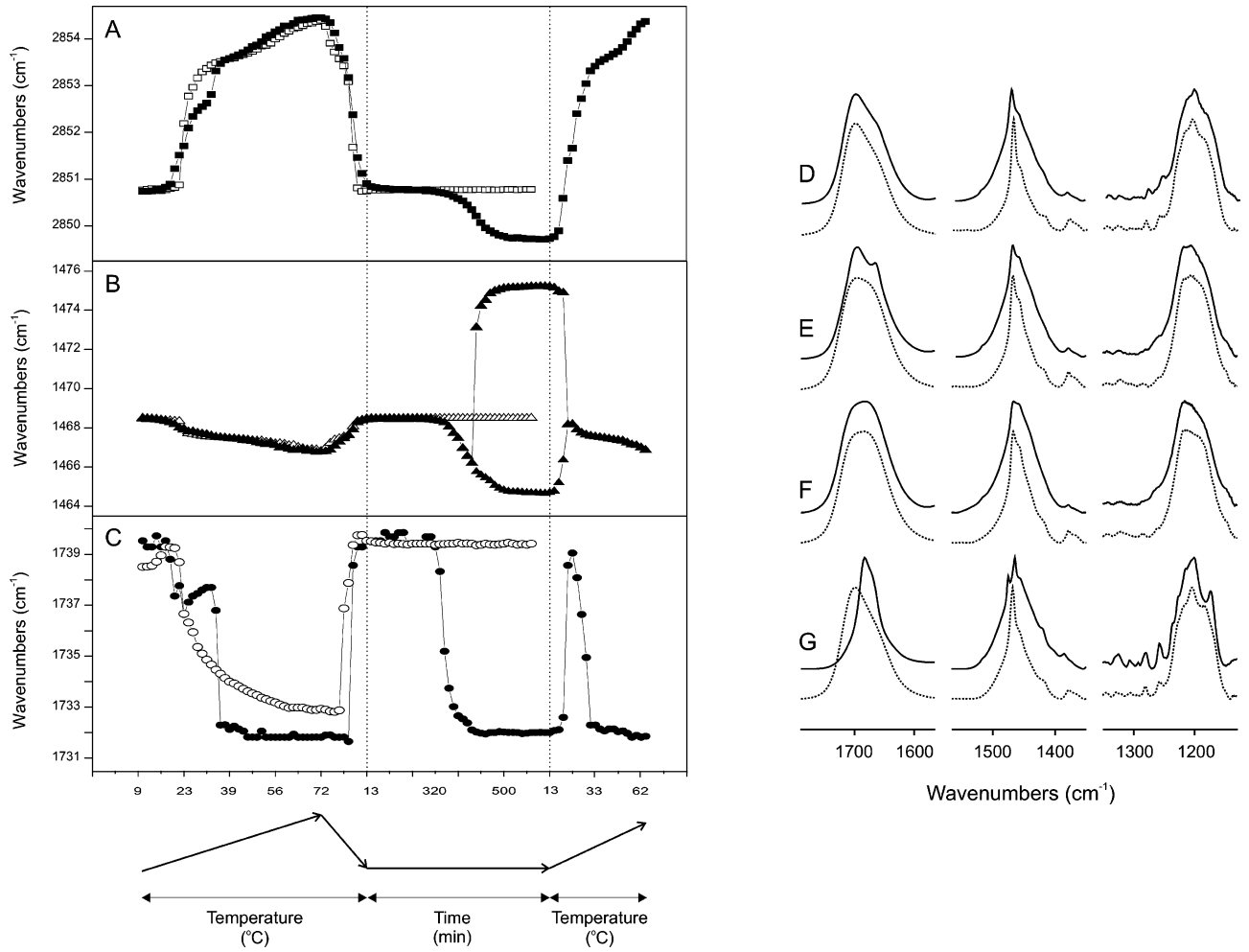

FIGURE 7: Temperature dependence of the maximum of the CH_2 symmetric stretching (A), C═O stretching (B), and CH_2 scissoring (C) vibration bands in the absence (□, △, ○) and in the presence (■, ▲, ●) of the gp41$^{568-588}$ peptide at a phospholipid-to-peptide molar ratio of 30:1. Scans were recorded at a regular interval of temperature from 9 to 72 °C, afterward allowed to cool until 10/13 °C, maintained at this temperature for 12 h, and heated again to 65 °C. Infrared spectra of the C═O, CH_2 scissoring, and PO_2^- stretching band regions of DMPG (···) and DMPG in the presence of the gp41$^{568-588}$ peptide (—) at 15 °C (D), 27 °C (E), and 46 °C (F) and incubated at 10/13 °C (G).

from what was observed for the pure phospholipid. At low temperatures, the C═O stretching band was similar to the C═O stretching band of the pure phospholipid. At increasing temperatures, the half-bandwidth of the C═O stretching band decreased, and two narrow bands were apparent; increasing the temperature, the two narrow bands combined and a similar broad C═O band to the pure phospholipid was apparent (Figure 6D). For the pure phospholipid, the half-bandwidth was about 33 and 38 cm^{-1} below and above the T_m; however, in the presence of the peptide the half-bandwidth of the C═O band was 36, 34, and 36 cm^{-1} below, between, and above the transitions, respectively. The frequency at the maximum of the C═O vibration band of DMPG in the presence of the gp41$^{568-588}$ peptide presented two well-defined transitions which corresponded to the three different C═O band envelopes observed previously in Figure 6D. This behavior is in accordance with the two overlapped transitions observed in the CH_2 stretching frequency of DMPG (Figure 5A). Therefore, the gp41$^{568-588}$ peptide induces the appearance of a new transition in DMPG, besides the gel and liquid crystalline phase transitions found in the pure phospholipid.

We have also studied the behavior of the broad C═O carbonyl band in the binary mixtures $DMPC_d$/DMPA and $DMPC_d$/DMPG (not shown for briefness). A single broad transition was observed for both types of samples, which were coincidental with the broad transitions observed for the CH_2 and CD_2 stretching frequencies of DMPG, DMPA, and $DMPC_d$ in the corresponding binary mixtures $DMPC_d$/DMPA and $DMPC_d$/DMPG (Figure 5C−F). No significant changes were observed either above or below the T_m of the mixtures.

A detailed study of the frequencies and envelopes of the CH_2 stretching, CH_2 scissoring,and C═O stretching vibration regions of DMPG at different incubation conditions both in the absence and in the presence of the gp41$^{568-588}$ peptide is presented in Figure 7. Upon increasing the temperature, it is possible to observe through the maximum of the CH_2 symmetric stretching vibration band the gel-to-liquid crystalline phase transition of the pure phospholipid at approximately 23 °C (Figure 7A). If the temperature is further increased, the frequency of the band increases progressively; if the system is allowed to cool, the liquid crystalline-to-gel phase transition takes place at approximately 23 °C. The characteristic gel state frequency is maintained even after incubation for several hours at low temperatures (Figure 7A). In the presence of the gp41$^{568-588}$ peptide and upon increasing the temperature, the maximum of the CH_2 symmetric stretching vibration band presents two transitions instead of

one as observed for the pure phospholipid (Figure 7A). The decrease in the CH_2 symmetric stretching band frequency upon incubation at low temperature indicates a further increase in the *trans* isomers of DMPG which was not observed for the pure phospholipid (Figure 7A). The behavior of the CH_2 scissoring band is similar to that found for the CH_2 stretching frequency, since the frequency maximum decreases slightly at the gel-to-liquid crystalline phase transition, decreases steadily as the temperature is increased, increases at the liquid crystalline-to-gel phase transition, and maintains after incubation for some hours at low temperature (Figure 7B). Significantly, and in the presence of the $gp41^{568-588}$ peptide, the CH_2 scissoring band splits in two bands upon incubation at low temperature (Figure 7B); however, and upon increasing the temperature, the splitted bands coalesce (Figure 7B). The maximum of the C═O stretching band of pure DMPG increases slightly at the pretransition, decreases at the gel-to-liquid crystalline phase transition, increases again as the temperature is lowered, and does not change upon incubation at low temperatures (Figure 7C). The most significant change of the maximum of the C═O vibration band in the presence of the $gp41^{568-588}$ peptide is the presence upon increasing the temperature of two transitions at about 21−22 and 33−36 °C as commented above (see Figure 7C). The new DMPG phase which appears between the $P_{\beta'}/L_{\beta'}$ and the L_α phases in the presence of the peptide has not been, to our knowledge, described until now.

The spectra shown in Figure 7D−G rationalize the behavior found for DMPG in the different conditions tested. At 15 °C and in the well-hydrated state, the different infrared regions corresponding to DPMG, both in the absence and in the presence of the gp41 peptide, present a typical envelope (Figure 7D). At 27 °C, the most important difference is found in the C═O stretching band of DMPG in the presence of the peptide, since two peaks are clearly resolved in contrast to the broad C═O band observed for the pure phospholipid (Figure 7E). Above 33 °C, both in the absence and in the presence of the peptide, the different regions of DMPG do not present any significant differences (Figure 7F). However, upon incubation at low temperatures, a narrow C═O band and a splitting in the CH_2 scissoring bands are found in the presence of the peptide (Figure 7G).

It is already known that, above 0 °C, well-hydrated pure DMPG at high ionic strength presents three different phases, i.e., the $P_{\beta'}$, $L_{\beta'}$, and L_α phases with corresponding transitions at 13−14 and 23−24 °C (*36*, *37*). The $P_{\beta'}$ and $L_{\beta'}$ phases are characterized by orientationally disordered *all-trans* chains and less mobile interfacial groups whereas the L_α phase is characterized by conformationally disordered chains and mobile well-hydrated interfacial groups (*37*). It is also known that DMPG, either at low ionic strength or in the presence of divalent cations, presents a complex polymorphic phase behavior which is dependent on acyl chain length and temperature (*36*−*38*). Apart from the $P_{\beta'}$, $L_{\beta'}$, and L_α phases, two more phases have been described for PGs containing saturated even-numbered acyl chains, the L_c2 and L_c1b phases (*36*−*38*). The L_c2 phase is a stable quasi-crystalline polymorph which appears upon long-term low-temperature incubation characterized by orientationally disordered *all-trans* chains and dehydrated and immobilized interfacial groups, whereas the L_c1b phase is a metastable quasi-crystalline phase characterized by orthorhombically packed *all-trans* chains and partially dehydrated and moderately immobile interfacial groups (*37*). The new DMPG phase which is found at low temperatures and in the presence of the peptide (see Figure 7) is characterized by a C═O stretching frequency maximum at 1732 cm^{-1} with components after deconvolution at 1732 and 1723 cm^{-1}, as well as a CH_2 scissoring band doublet with maxima at 1475 and 1464 cm^{-1}, whereas the sharp and equidistant methylene progression bands demonstrate that the acyl chains are in the *all-trans* conformation (*39*). These data are characteristic of the L_c1b phase (*37*). As observed in Figure 7E, this new phase presents a CH_2 scissoring and PO_2^- band envelopes similar to those found in the $P_{\beta'}/L_{\beta'}/L_\alpha$ phases of the pure phospholipid, so that the phospholipid probably presents orientationally and conformationally disordered chains along with hydrated mobile headgroups intermediate to those present in the $P_{\beta'}/L_{\beta'}$ and L_α phases. Incubation of DMPG at low temperatures in the presence of the peptide, so that the low-temperature metastable phase was induced, did not produce any change in the lifetimes of the peptide (see Table 2), which is in accordance with the infrared results which reflect that the peptide did not undergo any alteration in conformation when this metastable phase was induced.

DISCUSSION

Membrane fusion reactions are involved in many important biological processes, but strong hydration, steric and electrostatic, repulsion forces represent large energetic barriers (*40*). These obstacles are overcome in biological systems by specific fusion proteins, and the simplest membrane fusion biological process is the one produced by the entry of enveloped viruses into cells (*1*−*3*, *41*). However, very little is known about how the complex series of protein/protein and protein/phospholipid interactions drive membrane apposition and how they overcome the energy barriers for membrane fusion. Moreover, it is already known that different regions of fusion proteins, including the HIV gp41 ectodomain, are essential for membrane fusion to occur (*8*−*11*, *42*). Therefore, destabilization of the lipid bilayer and membrane fusion appears to be the result of the binding and interaction of different segments of fusion proteins with the biological membrane. Understanding the characteristic features that determine the specificity and stability of the native, metastable, and the fusogenic stable conformations is required for the understanding of the mechanism of viral membrane fusion (*41*). Many studies have been carried out on the interactions of synthetic peptides mimicking the N-terminal fusion peptide and the Trp-rich proximal membrane regions of gp41, but fewer ones have been done on the interaction of other segments of the gp41 protein with phospholipid model membranes. However, new targets for gp41-mediated membrane fusion may be uncovered by obtaining detailed structural information on both the native and fusion-intermediate conformations of gp41. In this study we have focused on the possible roles of a region pertaining to the NHR region in the membrane fusion process, since we have previously shown that different segments originating from this region have membrane-active properties (ref *7* and unpublished experiments).

The $gp41^{568-588}$ peptide we have studied in this work binds with high affinity to phospholipid model membranes, and upon binding, the peptide resides in an environment of low

dielectric constant showing a remarkable motional restriction as concluded from its anisotropy values. The peptide enters a hydrophobic environment but remains located at the surface of the membrane, as indicated by the effects observed on the frequency of the CH_2 and CD_2 stretching bands of the hydrocarbon chains of the phospholipids. The infrared spectra of the amide I′ region of the fully hydrated peptide in D_2O buffer indicate a high stability of its conformation in solution, even at high temperatures. However, when the peptide was bound to phospholipid model membranes, its conformation changed. More significant, the envelope of the amide I′ band of the peptide in the presence of DMPA changed its conformation depending on the phase transition of the phospholipid. The binding to the surface and the modulation of the phospholipid biophysical properties which take place when the peptide is bound to the membrane, i.e., partitioning into the membrane surface, aggregation and perturbation of the bilayer architecture, could be related to the conformational changes which occur upon binding of the HIV-1 gp41 glycoprotein to the host cell plasma membrane. Moreover, this peptide has the capacity of inducing membrane leakage and membrane hemifusion as well as is capable of autoaggregation as seen by time-resolved fluorescence. These data could suggest a tendency of the peptide to self-assemble, and probably these changes might be part of the structural transition that transforms gp41 from the inactive to the active state, the dominant form during membrane fusion (*2*, *4*). The gp41 peptide fragment we have studied here binds, interacts, and perturbs phospholipid model membranes and at the same time changes its conformation in a membranous environment. These conformational changes are reversible, suggesting that the peptide conformation is significantly altered by the phospholipid phase transition.

Membrane lipids undergo a cooperative melting reaction, which is linked to the loss of conformational order of the lipid chains, and it has been known for a long time that the melting process of membrane lipids is influenced by many types of molecules including proteins and peptides. Phosphatidylglycerol (PG), one of the most studied naturally occurring anionic phospholipids, is more sensitive to factors such as pH, ionic strength, and divalent cations than zwitterionic phospholipids. Also, DMPG, which under well-hydrated conditions presents a gel-to-liquid crystalline phase transition at 23 °C, is commonly used in biophysical studies of negatively charged model membrane systems (*37*, *43*−*45*). Even under physiologically relevant conditions, PGs can exhibit a more complex pattern of thermotropic phase behavior than the corresponding PCs, which could include the formation of one or more high-melting crystalline or quasi-crystalline lamellar phases and the formation of extended three-dimensional bilayer networks where curvature elasticity is of primary relevance (*36*, *46*). The pattern of thermotropic phase behavior exhibited by freshly dispersed samples of these PGs is remarkably similar to that of the corresponding 1,2-diacyl-PCs (*37*). However, incubation of PGs at low temperatures results in the formation of one or more quasi-crystalline structures at rates dependent on the hydrocarbon chain length. For example, DMPG incubated at low temperatures for extended periods of time forms a metastable quasi-crystalline phase designated as the L_c1b phase, while longer time incubation gives place to a stable high-melting polymorph designated as L_c2 (*38*, *46*). The gp41 peptide we have studied here, after binding to DMPG, is capable of easily inducing the L_c1b phase at low temperatures and, more significantly, a new phase at intermediate ones. Therefore, it can be supposed that these interactions might have large implications for different biological processes and particularly to membrane perturbation.

It has been previously suggested that gp41 hairpin folding drives the fusion reaction by initiating pore formation, but it has been also recently shown that fusion pore formation might occur prior to hairpin formation and that hairpin formation might be required for pore stabilization (*47*). Folding to a hairpin would bring the apposing membranes together, align the target membrane fusion domains with the transmembrane region of the viral envelope, and would imply a direct interaction of the two membrane proximal regions with their respective membrane targets (*2*, *11*). Since membrane fusion can be described by a succession of steps, i.e., apposition of membranes, hemifusion of the outer leaflets, pore formation, and pore enlargement, exposed regions of the prehairpin intermediates should be those responsible for the first steps of fusion until pore initiation occurs. It should be borne in mind that it has been suggested that, in the case of the formation of circular pores, there is a critical pore radius, below which individual pores reseal and above which there is a coalescence into a single large hole; instability arises from fluctuations of hole size (*40*). Moreover, the opening of aqueous pores and/or disruption effects might be of biological relevance, and this phenomenon might be characteristic not only for PG-containing membranes but also for negative phospholipid- containing membranes in general. Indeed, a high local concentration of specific phospholipid types could help the formation and stabilization of transient disruption effects which could be essential for biological processes such as membrane fusion. The reversible formation of high-viscosity extended three-dimensional phases might be a rather general phenomenon which might be triggered by, for example, external factors such as protein binding in conditions which favor positive membrane curvature. These processes might be essential for membrane fusion in biological membranes. HIV-induced membrane fusion is considered as an attractive target for chemotherapeutic intervention, as blocking virus entry leads to suppression of viral infectivity, replication, and the cytotoxicity induced by virus cell contacts. The inhibition of membrane fusion by direct action on gp120 and/or gp41 is increasing in importance as an additional approach either to combat directly against HIV infection or to prevent its spread, and an understanding of the structural features of their intermediates is essential because it appears to be an attractive drug target. The results reported in this work sustain the notion that different specific regions of gp41 are capable of modifying the biophysical properties of phospholipid membranes, a property which might provide an additional driving force for the merging of the viral and host cell membranes and, therefore, might be essential for the assistance and enhancement of the viral and cell fusion process.

ACKNOWLEDGMENT

We thank María T. Garzón and Mónica García for excellent technical assistance.

REFERENCES

1. Eckert, D. M., and Kim, P. S. (2001) Mechanisms of viral membrane fusion and its inhibition, *Annu. Rev. Biochem. 70*, 777−810.
2. Gallo, S. A., Finnegan, C. M., Viard, M., Raviv, Y., Dimitrov, A., Rawat, S. S., Puri, A., Durell, S., and Blumenthal, R. (2003) The HIV Env-mediated fusion reaction, *Biochim. Biophys. Acta 1614*, 36−50.
3. Markovic, I., and Clouse, K. A. (2004) Recent advances in understanding the molecular mechanisms of HIV-1 entry and fusion, revisiting current targets and considering new options for therapeutic intervention, *Curr. HIV Res. 2*, 223−234.
4. Dimitrov, A. S., Xiao, X., Dimitrov, D. S., and Blumenthal, R. (2000) Early intermediates in HIV-1 envelope glycoprotein-mediated fusion triggered by CD4 and co-receptor complexes, *J. Biol. Chem. 276*, 30335−30341.
5. Bosch, M. L., Earl, P. L., Fargnoli, K., Picciafuoco, S., Giombini, F., Wong-Staal, F., and Franchini, G. (1989) Identification of the fusion peptide of primate immunodeficiency viruses, *Science 244*, 694−697.
6. Gallaher, W. R., Ball, J. M., Garry, R. F., Griffin, M. C., and Montelaro, R. C. (1989) A general model for the transmembrane proteins of HIV and other retroviruses, *AIDS Res. Hum. Retroviruses 5*, 431−440.
7. Moreno, M. R., Pascual, R., and Villalaín, J. (2004) Identification of membrane-active regions of the HIV-1 envelope glycoprotein gp41 using a 15-mer gp41-peptide scan, *Biochim. Biophys. Acta 1661*, 97−105.
8. Pascual, R., Moreno, M. R., and Villalaín, J. (2005) A peptide pertaining to the loop-segment of HIV gp41 binds and interacts with model biomembranes. Implications on the fusion mechanism, *J. Virol. 79*, 5142−5152.
9. Suárez, T., Nir, S., Goñi, F. M., Sáez-Cirión, A., and Nieva, J. L. (2000) The pre-transmembrane region of the human immunodeficiency virus type-1 glycoprotein, a novel fusogenic sequence, *FEBS Lett. 477*, 145−149.
10. Contreras, L. M., Aranda, F. J., Gavilanes, F., González-Ros, J. M., and Villalaín, J. (2001) Structure and interaction with membrane model systems of a peptide derived from the major epitope region of HIV protein gp41: implications on viral fusion mechanism, *Biochemistry 40*, 3196−3207.
11. Dimitrov, A. S., Rawat, S. S., Jiang, S., and Blumenthal, R. (2003) Role of the fusion peptide and membrane-proximal domain in HIV-1 envelope glycoprotein-mediated membrane fusion, *Biochemistry 42*, 14150−14158.
12. Peisajovich, S. G., Epand, R. F., Pritsker, M., Shai, Y., and Epand, R. M. (2000) The polar region consecutive to the fusion peptide participates in membrane fusion, *Biochemistry 39*, 1826−1833.
13. Sackett, K., and Shai, Y. (2002) The HIV-1 gp41 N-terminal heptad repeat plays an essential role in membrane fusion, *Biochemistry 41*, 4678−4685.
14. Lakey, J. H., Parker, M. W., Gonzalez-Mañas, J. M., Duche, D., Vriend, G., Baty, D., and Pattus, F. (1994) The role of electrostatic charge in the membrane insertion of colicin A. Calculation and mutation, *Eur. J. Biochem. 220*, 155−163.
15. Pinheiro, T. J., and Watts, A. (1994) Lipid specificity in the interaction of cytochrome *c* with anionic phospholipid bilayers revealed by solid-state 31P NMR, *Biochemistry 33*, 2451−2458.
16. Liu, L. P., and Deber, C. M. (1997) Anionic phospholipids modulate peptide insertion into membranes, *Biochemistry 36*, 5476−5482.
17. Earp, L. J., Delos, S. E., Park, H. E., and White, J. M. (2005) The many mechanisms of viral membrane fusion proteins, *Curr. Top. Microbiol. Immunol. 285*, 25−66.
18. Surewicz, W. K., Mantsch, H. H., and Chapman, D. (1993) Determination of protein secondary structure by Fourier transform infrared spectroscopy: a critical assessment, *Biochemistry 32*, 389−394.
19. Zhang, T. P., Lewis, R. N. A. H., Hodges, R. S., and McElhaney, R. N. (1992) FTIR spectroscopic studies of the conformation and amide hydrogen exchange of a peptide model of the hydrophobic transmembrane alpha-helices of membrane proteins, *Biochemistry 31*, 11572−11588.
20. Szoka, F., Jr., and Papahadjopoulos, D. (1980) Comparative properties and methods of preparation of lipid vesicles (liposomes), *Annu. Rev. Biophys. Bioeng. 9*, 467−508.
21. Hope, M. J., Bally, M. B., Webb, G., and Cullis, P. R. (1985) Production of large unilamellar vesicles by a rapid extrusion procedure. Characterization of size distribution, trapped volume and ability to maintain a membrane potential, *Biochim. Biophys. Acta 812*, 55−65.
22. Böttcher, C. J. F., Van Gent, C. M., and Pries, C. (1961) A rapid and sensitive sub-micro phosphorus determination, *Anal. Chim. Acta 24*, 203−204.
23. Edelhoch, H. (1967) Spectroscopic determination of tryptophan and tyrosine in proteins, *Biochemistry 6*, 1948−1954.
24. Giudici, M., Pascual, R., de la Canal, L., Pfüller, K., Pfüller, U., and Villalaín, J. (2003) Interaction of viscotoxins A_3 and B with membrane model systems: implications to their mechanism of action, *Biophys. J. 85*, 971−981.
25. Kauppinen, J. K., Moffatt, D. J., Mantsch, H. H., and Cameron, D. G. (1981) Fourier selfdeconvolution: a method for resolving intrinsically overlapped bands, *Appl. Spectrosc. 35*, 271−276.
26. Mantsch, H. H., Moffatt, D. J., and Casal, H. (1988) Fourier transform methods for spectral resolution enhancement, *J. Mol. Struct. 173*, 285−298.
27. Bañuelos, S., Arrondo, J. L. R., Goñi, F. M., and Pifat, G. (1995) Fourier transform methods for spectral resolution enhancement, *J. Biol. Chem. 270*, 9192−9196.
28. Struck, D. K., Hoekstra, D., and Pagano, R. E. (1981) Use of resonance energy transfer to monitor membrane fusion, *Biochemistry 20*, 4093−4099.
29. Loura, L. M., Fedorov, A., and Prieto, M. (1996) Resonance energy transfer in a model system of membranes: application to gel and liquid crystalline phases, *Biophys. J. 71*, 1823−1836.
30. Lakowicz, J. R. (1999) *Principles of fluorescence spectroscopy*, 2nd ed., Plenum Press, New York.
31. Santos, N. C., Prieto, M., and Castanho, M. A. (1998) Interaction of the major epitope region of HIV protein gp41 with membrane model systems. A fluorescence study, *Biochemistry 37*, 8674−8682.
32. Arrondo, J. L. R., and Goñi, F. M. (1999) Structure and dynamics of membrane proteins as studied by infrared spectroscopy, *Prog. Biophys. Mol. Biol. 72*, 367−405.
33. Paré, Ch., Lafleur, M., Liu, F., Lewis, R. N. A., and McElhaney, R. N. (2001) Differential scanning calorimetry and ^{2}H nuclear magnetic resonance and Fourier transform infrared spectroscopic studies of the effects of transmembrane α-helical peptides on the organization of phosphatidylcholine bilayers, *Biochim. Biophys. Acta 1511*, 60−73.
34. Mantsch, H. H., and McElhaney, E. N. (1991) Phospholipid phase transitions in model and biological membranes as studied by infrared spectroscopy, *Chem. Phys. Lipids 57*, 213−226.
35. Blüme, A., Hübner, W., and Messner, G. (1988) Fourier transform infrared spectroscopy of ^{13}C═O-labeled phospholipids hydrogen bonding to carbonyl groups, *Biochemistry 27*, 8239−8249.
36. Lamy-Freund, M. T., and Riske, K. A. (2003) The peculiar thermo-structural behavior of the anionic lipid DMPG, *Chem. Phys. Lipids 122*, 19−32.
37. Zhang, Y. P., Lewis, R. N. A. H., and McElhaney, R. N. (1997) Calorimetric and spectroscopic studies of the thermotropic phase behavior of the n-saturated 1,2-diacylphosphatidylglycerols, *Biophys. J. 72*, 779−793.
38. Garidel, P., Blume, A., and Hübner, W. (2000) A Fourier transform infrared spectroscopic study of the interaction of alkaline earth cations with the negatively charged phospholipid 1,2-dimyristoyl-*sn*-glycero-3-phosphoglycerol, *Biochim. Biophys. Acta 1466*, 245−259.
39. Casal, H. L., and Mantsch, H. H. (1984) Polymorphic phase behaviour of phospholipid membranes studied by infrared spectroscopy, *Biochim. Biophys. Acta 779*, 381−401.
40. Chernomordik, L. V., and Kozlov, M. M. (2003) Protein−lipid interplay in fusion and fission of biological membranes, *Annu. Rev. Biochem. 72*, 175−207.
41. Blumenthal, R., Clague, M. J., Durell, S. R., and Epand, R. M. (2003) Membrane fusion, *Chem. Rev. 103*, 53−69.
42. Salzwedel, K., West, J. T., and Hunter, E. (1999) A conserved tryptophan-rich motif in the membrane-proximal region of the human immunodeficiency virus type 1 gp41 ectodomain is important for env-mediated fusion and virus infectivity, *J. Virol. 73*, 2469−2480.
43. Heimburg, T., and Biltonen, R. L. (1994) Thermotropic behavior of dimyristoylphosphatidylglycerol and its interaction with cytochrome *c*, *Biochemistry 33*, 9477−9488.

44. Prenner, E. J., Lewis, R. N., Kondejewski, L. H., Hodges, R. S., and McElhaney, R. N. (1999) Differential scanning calorimetric study of the effect of the antimicrobial peptide gramicidin S on the thermotropic phase behavior of phosphatidylcholine, phosphatidylethanolamine and phosphatidylglycerol lipid bilayer membranes, *Biochim. Biophys. Acta 1417*, 211−223.
45. Liu, F., Lewis, R. N., Hodges, R. S., and McElhaney, R. N. (2004) Effect of variations in the structure of a polyleucine-based α-helical transmembrane peptide on its interaction with phosphatidylglycerol bilayers, *Biochemistry 43*, 3679−3687.
46. Epand, R. M., Gabel, B., Epand, R. F., Sen, A., Hui, S. W., Muga, A., and Surewicz, W. K. (1992) Formation of a new stable phase of phosphatidylglycerols, *Biophys. J. 63*, 327−332.
47. Markosyan, R. M., Cohen, F. S., and Melikyan, G. B. (2003) HIV-1 envelope proteins complete their folding into six-helix bundles immediately after fusion pore formation, *Mol. Biol. Cell 14*, 926−938.

BI050928+